Journal of Sound and Vibration 329 (2010) 5415–5433

Contents lists available at ScienceDirect

Journal of Sound and Vibration

journal homepage: www.elsevier.com/locate/jsvi

Studies of the performance of particle dampers under dynamic loads

Zheng Lu [a], Xilin Lu [a,*], Sami F. Masri [b]

[a] State Key Laboratory of Disaster Reduction in CivilEngineering, Tongji University, Shanghai 200092, China
[b] Viterbi School of Engineering, University of Southern California, Los Angeles, California 90089-2531, USA

ARTICLE INFO

Article history:
Received 26 December 2009
Received in revised form
23 March 2010
Accepted 20 June 2010
Handling Editor: L.G. Tham
Available online 7 August 2010

ABSTRACT

This paper presents a systematic investigation of the performance of particle dampers (vertical and horizontal) attached to a primary system (single-degree-of-freedom (SDOF) and multi-degree-of-freedom (MDOF)) under different dynamic loads (free vibration, stationary random excitation as well as nonstationary random excitation, with single component or multi-component), and the optimum operating regions are all determined. The amount of dissipated energy due to impact and friction, and the concept of "*Effective Momentum Exchange*" are shown to be suitable "global" measures to interpret the physics involved in the behavior of particle dampers. Using the well-established discrete element method, the motion of vertical particle dampers can be analyzed and classified into three different regions, and the associated damping characteristics can be interpreted. The first mode of a MDOF primary system can be effectively controlled by a properly designed particle damper; however, the higher modes are more affected by other parameters. Consequently, extensive parametric studies are presented to evaluate the effects of various system parameters, such as: mass ratio, primary system damping, coefficient of restitution, container dimensions, excitation amplitude and components, input locations and damper locations.

1. Introduction

1.1. Background

Structural control plays a very important role in engineering and can be divided into three categories, namely passive, active and hybrid control techniques, in which the passive strategy is most widely applied. Among numerous passive devices for structural control applications (see, e.g. the works of Zhao [1], Franchek et al. [2], Gardonio and Elliott [3], and Guyomar and Badel [4]), a class of highly nonlinear dampers (particle dampers) that simultaneously utilize momentum transfer and internal energy dissipation offer some advantages in practical situations. Particle dampers, which evolved from the single-particle impact damper (Masri and Caughey [5]), are containers or structural voids partially filled with particles (e.g., ball bearings, tungsten powders, etc.). With the advantages of ruggedness, reliability, and insensitivity to extreme temperatures, these simple and efficient passive devices are used to attenuate the vibrations of lightly damped structures, especially in harsh environments where traditional approaches fail.

There is a long history of research in the modeling, analysis, simulation, design and deployment of this class of vibration control devices. The first practical application of an impact damper was reported by Paget [6], where impact dampers were

* Corresponding author. Tel.: +86 21 65983430; fax: +86 21 65982668.
E-mail addresses: luzheng111@gmail.com (Z. Lu), lxlst@tongji.edu.cn (X. Lu), masri@usc.edu (S.F. Masri).

0022-460X/$ - see front matter © 2010 Elsevier Ltd. All rights reserved.
doi:10.1016/j.jsv.2010.06.027

Nomenclature

A_0	initial displacement under free vibration
c_2	damping constant of impact damper "stops"
c_3	damping constant of the damper between two particles
C_i	damping constant of ith floor
$\mathbf{C}$	damping matrix of the primary system
d	diameter of a particle
dx	length of the container
dy	width of the container
dz	height of the container
e	coefficient of restitution
E	dissipated energy due to impact and friction
E_e	energy of the excitation force
$\mathbf{E}$	matrix induced ground acceleration
F_i	contact force between ith floor and particle container
$\mathbf{F}$	matrix of contact force between the primary system and particle container
$\mathbf{F}_{ij}^n$	normal contact force between particle i and particle j
$\mathbf{F}_{ij}^t$	tangential contact force between particle i and particle j
$g(t)$	deterministic envelope function
$\mathbf{g}$	acceleration vector due to gravity
$\mathbf{I_i}$	moment of inertia of particle i
k_2	stiffness of the impact damper "stops"
k_3	stiffness of the spring between two particles
k_i	number of contact particles that are in contact with particle i
K_i	equivalent stiffness of ith floor
$\mathbf{K}$	equivalent stiffness matrix of the primary system
m_i	mass of the particle i
M_e	momentum exchange of the excitation force
M_i	mass of ith floor
$\mathbf{M}$	mass matrix of the primary system
$n(t)$	stationary random excitation
$\mathbf{n}_{ij}$	unit vector from the center of particle i to the center of particle j
N	total number of the particles
$\mathbf{p}_i$	position vector of the center of gravity of particle i
$s(t)$	resulting nonstationary random excitation, $s(t)=g(t)n(t)$
$\mathbf{T}_{ij}$	torque between particle i and particle j
$\ddot{x}_g$	ground acceleration
X_i	relative displacement of ith floor with respect to the ground
Z_{st}	static deflection
δ_n	normal relative displacement
$\dot{\delta}_n$	normal relative velocity
$\dot{\delta}_t$	tangential relative velocity
Δ_i	distance from the center of particle i to the wall
ζ	damping ratio of the primary system
ζ_2	damping ratio of impact damper "stops"
ζ_3	damping ratio of the damper between two particles
μ	mass ratio, which is the ratio of the total mass of particles and the total mass of the primary system
μ_s	coefficient of friction
σ_r	root-mean-square value of the displacement of the primary system with a particle damper
σ_{r0}	root-mean-square value of the displacement of the primary system without a particle damper
$\boldsymbol{\varphi}_i$	angular displacement vector of particle i
ω_2	natural frequency of the impact damper "stops"
ω_3	natural frequency of the spring between two particles
ω_n	natural frequency of the primary system

employed to control the vibration of turbine blades. Theoretical studies of impact dampers oriented by considering only perfect plastic impacts, as descried by Lieber [7], and by an assumption of steady state motion with two equispaced impacts per cycle. Masri [8–10] gave a closed solution for the steady-state motion of a multi-unit impact damper attached to a periodically excited primary system. Bapat and Sankar [11] studied the effect of Coulomb friction on the performance of identical multi-unit impact damper and Bapat [12] further developed nonlinear equations governing N impacts per cycle of a single-degree-of-freedom (SDOF) oscillator under a sinusoidal excitation. Popplewell and Semercigil [13] compared the performance of a resilient bean bag (a plastic bag filled with lead shots) and a conventional rigid impact damper under sinusoidal excitation. Bryce et al. [14] discussed the effectiveness and predictability of particle dampers, and also developed a complete design methodology which had been validated in laboratory studies. Bai et al. [15] proposed and investigated the behavior of a piston-based particle damper.

Many experimental studies and numerical simulations have been carried out for the characterization of particle dampers. Thomas [16] tested an impact damper used to improve the chatter performance of a cantilever boring bar. Ema and Marui [17] carried out a fundamental experimental study on impact dampers and achieved the optimum damping effect by adjusting the mass ratio and clearance. Michael et al. [18] developed a pair of two-dimensional master design curves with unitless axes which are comprised of combinations of design parameters. Li [19] conducted a series of experimental investigations to find out the effect of an impact damper on a multi-degree-of-freedom (MDOF) system.

As to numerical simulations, Papalou and Masri [20–22] introduced an equivalent single-particle impact damper model to evaluate the performance of multi-particle dampers. Liu et al. [23] used an equivalent viscous damping model to represent the nonlinearity which was extracted from experimental results. Xu et al. [24] presented an empirical method for particle damping design. Fang and Tang [25] developed an improved analytical model by multiphase flow theory based on

the previous work of Wu et al. [26]. Although these equivalent models or empirical-based studies have given many new insights, they are essentially phenomenological, and the results are difficult to extrapolate beyond their respective experimental conditions. Recently, the discrete-element method (DEM), which can take interactions between particles into account, has been used to perform limited studies of particle dampers (Saeki [27,28], Mao et al. [29], Hu [30], and Wong et al. [31]).

Despite all these efforts, the understanding of the particle damping mechanism has still not been well developed, due to the system's high nonlinearity and the complexity involving interactions among a large number of parameters. It can be seen that most of the studies listed above have investigated the interaction between a particle damper (or an impact damper) and a SDOF primary structure. The performance of particle dampers with MDOF primary system has seldom been investigated. Moreover, the behavior of particle dampers in their optimum operating regions are not thoroughly studied, either. Also, due to the gravity field, the performance of particle dampers under vertical load needs further studies. Additionally, many parameters influence the behavior of particle dampers; however, it is not feasible to investigate the numerous particle damper design parameters experimentally. Consequently, there is a need for a comprehensive study of the performance of particle dampers when operating with a MDOF system that is subjected to dynamic loads.

1.2. Scope

This paper numerically investigates the performance of particle dampers (vertical and horizontal) attached to a primary system (SDOF and MDOF) under different dynamic loads (free vibration, stationary random excitation as well as nonstationary random excitation), with the aim of finding efficient ways to better characterize the particle damper behavior. The amount of dissipated energy, and the concept of *Effective Momentum Exchange* are used to characterize some of the physics underlying the operation of particle dampers.

The contents of this paper are arranged from a simple case to a more complicated case. For example, the primary system is arranged from SDOF to MDOF, the particle damper is employed from vertical direction to horizontal direction, and the dynamic loads are used from free vibration to random excitation, from uniaxial direction to multi directions. In detail, Section 2 presents the model of a vertical particle damper attached to a SDOF system, the model of a horizontal particle damper attached to a SDOF system, and the model of a particle damper attached to a MDOF system. The governing equations of motion for a particle damper system in three dimensions and a simulation program based on DEM are introduced. In Section 3, the performance of a vertical particle damper under free vibration is analyzed. Section 4 studies the behavior of a particle damper with a SDOF system under multi-component random excitations. The influences of the amount of dissipated energy and the *Effective Momentum Exchange* on the primary system under optimum operating conditions are also investigated. Section 5 studies the performance of a particle damper attached to a MDOF system and carries out parametric studies to get a better understanding of this nonlinear device. The parameters include mass ratio, coefficient of restitution, excitation levels, damping ratio of the primary system, container dimensions, and particle damper location.

2. Simulation method

The simplified model shown in Fig. 1(a) represents a primary system equipped with a vertical particle damper, Fig. 1(c) represents a primary system equipped with a horizontal particle damper, and Fig. 1(b) represents an N-storey shear building system equipped with an auxiliary nonlinear particle damper at the top floor, in which a certain number of particles are placed. As the simulation methods of these three models are similar, the MDOF system with a particle damper model is discussed below as an illustration.

The equations of motion of the primary system can be written as

$$\mathbf{M}\ddot{\mathbf{X}}+\mathbf{C}\dot{\mathbf{X}}+\mathbf{K}\mathbf{X}=\mathbf{F}+\mathbf{E}\ddot{x}_g \tag{1}$$

$$\mathbf{M}=diag[M_1\ \ M_2\ \ \ldots\ \ M_N] \tag{2}$$

$$\mathbf{C}=\begin{bmatrix}(C_1+C_2) & -C_2 & & & \\ -C_2 & (C_2+C_3) & -C_3 & & \\ & & & \ddots & -C_N \\ & & & -C_N & C_N\end{bmatrix} \tag{3}$$

$$\mathbf{K}=\begin{bmatrix}(K_1+K_2) & -K_2 & & & \\ -K_2 & (K_2+K_3) & -K_3 & & \\ & & & \ddots & -K_N \\ & & & -K_N & K_N\end{bmatrix} \tag{4}$$

$$\mathbf{X}=[X_1\ \ X_2\ \ \ldots\ \ X_N]^{\mathrm{T}} \tag{5}$$

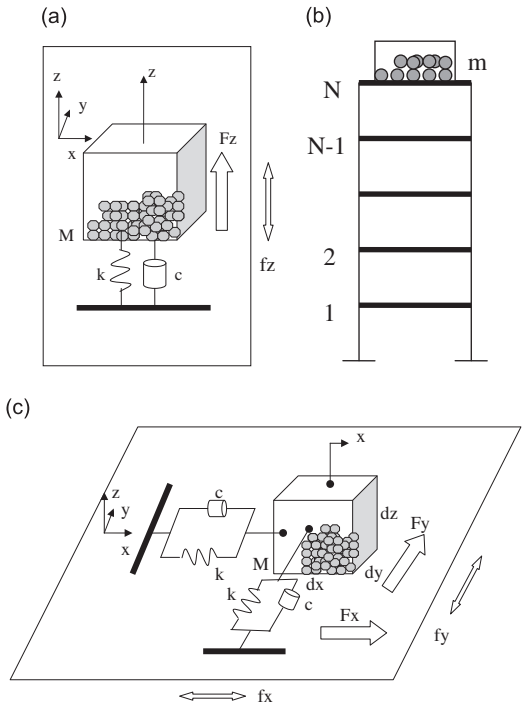

Fig. 1. (a) Model of a SDOF system with a vertical particle damper; (b) Model of a N-storey shear building system with a horizontal particle damper; (c) Model of a SDOF system with a horizontal particle damper.

$$\mathbf{F} = [0 \;\; 0 \;\; \ldots \;\; F_N]^{\mathrm{T}} \tag{6}$$

$$\mathbf{E} = [-M_1 \;\; -M_2 \;\; \ldots \;\; -M_N]^{\mathrm{T}} \tag{7}$$

where **M**, **C**, **K** are mass, damping, and stiffness matrices, respectively; **F**, **E**, and $\ddot{x}_g$ are the contact force vector, matrix induced ground acceleration, and ground acceleration, respectively. X_i is the relative displacement of the ith floor with respect to the ground; M_i, C_i, K_i are the mass, damping and stiffness of the ith floor, respectively; and F_i is the contact force acting on the ith floor by particles (i =1,2,…,N), which is the linkage between particles and the primary system.

The discrete-element method (Cundall [32]) is a numerical scheme that allows finite rotations and displacements of discrete bodies which are interacting according to local Contact laws, and are described by Newton's equations of motion. It is based on the idea that the time step chosen may be so small that, during a single time step, disturbances cannot propagate from any particle further than its immediate neighbors. Then, at all times, the forces acting on any particle are determined exclusively by its interaction with the particles with which it is in contact. This method is applied in this study to capture the behavior of the entire system in detail. With this technique, the position and contact force of the individual particle and the primary system can be traced at every single time step. As it is a macroscopic problem, molecular level forces (i.e., the Coulomb force and van der Waals force) are not considered; consequently, the governing equation for a particle i can be written as

$$m_i \ddot{\mathbf{p}}_i = m_i \mathbf{g} + \sum_{j=1}^{k_i} (\mathbf{F}_{ij}^n + \mathbf{F}_{ij}^t) \tag{8}$$

$$\mathbf{I}_i \ddot{\boldsymbol{\varphi}}_i = \sum_{j=1}^{k_i} \mathbf{T}_{ij} \tag{9}$$

where m_i is the mass of particle i, $\mathbf{I_i}$ is the moment of inertia of particle i and $\mathbf{g}$ is the acceleration vector due to gravity; $\mathbf{p}_i$ is the position vector of the center of gravity of particle i, $\boldsymbol{\varphi}_i$ is the angular displacement vector, $\mathbf{F}_{ij}^n$ is the normal contact force betweenparticles i and j (if particle i is in contact with container wall, then j denotes that wall) and $\mathbf{F}_{ij}^t$ is the tangential contact force. The contact forces act at the contact point between particles i and j rather than the particle center, and they will generate a torque, $\mathbf{T}_{ij}$, causing particle i to rotate. For a spherical particle of radius r_i, $\mathbf{T}_{ij}$ is given by $\mathbf{T}_{ij} = r_i \mathbf{n}_{ij} \times \mathbf{F}_{ij}^t$, where $\mathbf{n}_{ij}$ is the unit vector from the center of particles i to the center of particle j and $\times$ denotes the cross product. These inter-particle forces are summed over the k_i particles in contact with particle i.

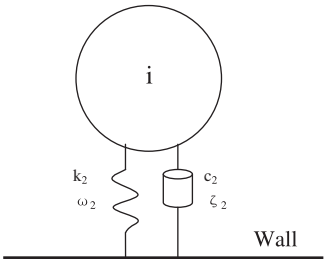

Fig. 2. Normal contact force model between a particle and the wall.

A number of contact models can be used to quantify the normal and tangential contact forces; however, this is still an active research topic, particularly for the tangential forces (Du and Wang [33]; Elperin and Golshtein [34]; Renzo and Maio [35]). The present simulation study uses a linear contact model in the normal direction, and Coulomb's law of friction in the tangential direction.

Fig. 2 presents the linear contact model between the particle and the wall in the normal direction, where a stiff spring and a viscous dashpot are acted in parallel to simulate the contact force. k_2 and c_2 are the stiffness and the damping constant of the impact damper "stops", respectively ("stops" are used here to name the combined mechanics of the spring and the dashpot between the particle and the wall [36]). $\omega_2=\sqrt{k_2/m}$ is the natural frequency, which can be used to simulate a rigid barrier to any degree of accuracy, by a proper choice. Based on previous studies (Masri [37]), the ratio of $\omega_2/\omega_n \geq 20$ is appropriate to represent a "stiff" barrier (ω_n is the natural frequency of the primary system). The parameter $\zeta_2=c_2/2m\omega_2$ is the damping ratio, which can be used to simulate inelastic impacts, ranging from the completely plastic up to the elastic one, so that a value of any desired coefficient of restitution e can be selected by adjusting the proper value for ζ_2. Similarly, k_3, ω_3, c_3 and ζ_3 are the stiffness, natural frequency of the spring, and the damping coefficient and damping ratio of the damper, respectively, in the inter-particle contact model along the normal direction. Hence, the normal contact force is expressed by

$$F_{ij}^n=\begin{cases} k_2\delta_n+2\zeta_2\sqrt{mk_2}\dot{\delta}_n & \delta_n=r_i-\Delta_i \quad \text{(particle}-\text{wall)} \\ k_3\delta_n+2\zeta_3\sqrt{\dfrac{m_im_j}{m_i+m_j}k_3}\dot{\delta}_n & \delta_n=r_i+r_j-|\mathbf{p}_j-\mathbf{p}_i| \quad \text{(particle}-\text{particle)} \end{cases} \tag{10}$$

where δ_n and $\dot{\delta}_n$ are the displacement and velocity of particle i relative to particle j, respectively, and Δ_i is the distance from the center of particle i to the wall.

Considering Coulomb's law of friction, the tangential contact force is expressed by

$$F_{ij}^t=-\mu_s F_{ij}^n\dot{\delta}_t/|\dot{\delta}_t| \tag{11}$$

where μ_s is the coefficient of friction between any two particles or between a particle and the wall of the container, and $\dot{\delta}_t$ is the velocity of particle i relative to particle j or the wall, in the tangential direction.

With the above in mind, the procedure for calculating the response of the particle dampers used in this study can now be illustrated. First, consider the relative position of the particles and walls. If $\delta_n>0$, the contact force acting on the particle can be determined from Eqs. (10) and (11); while if $\delta_n\leq 0$, no contact force is produced. Second, sum all the contact forces acting on this particle, including inter-particle forces and particle–wall forces, if they exist. Third, the particle motion can be analyzed by Eqs. (8) and (9). The same procedure is repeated for all the particles. Finally, the component of the contact force **F** acting on the primary system are given by the summation of all the contact forces between the particles and the wall of the container, respectively. By using the components of the contact force **F**, the equation of motion for the primary system, Eq. (1) is updated. One thing needs to be mentioned is that the DEM models of the particle are related to the building model by **F**, so this is an important quantity in the physical nature of the performance of particle dampers, and will be discussed in Section 4 in detail.

As a part of the study reported herein, a code was programmed, validated and implemented according to the above-mentioned procedure, and the fourth-order *Runge–Kutta* method was applied to solve the resulting system of nonlinear ordinary differential equations [38].

3. A vertical particle damper with a SDOF system under free vibration

In this section, the performance of a vertical rectangular particle damper attached to a SDOF system under free vibration is studied. The model can be found in Fig. 1(a). Friend [39] presented experimental tests of a SDOF system with a particle vibration damper by embedding metal particles in a closure attached to the end of a beam. The primary system natural frequency is 17.8 Hz, the mass is 0.0376 kg, the damping ratio is 0.012, and the coefficient of friction is 0.55. The particle damper is composed of 512 metal particles with a total mass of 0.004 kg, each with a diameter (d) of 1.2 mm, and a coefficient of restitution (e) of 0.75.

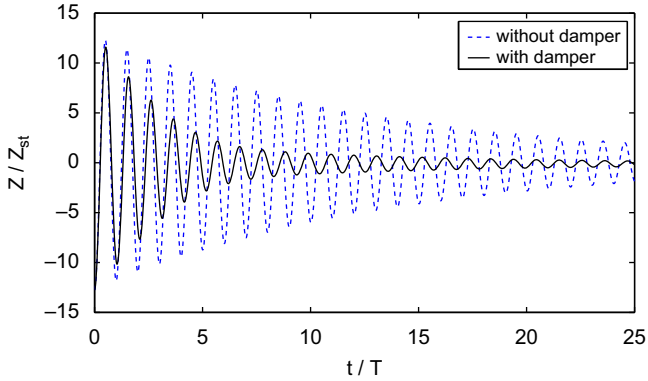

Fig. 3. Free vibration displacement time history of the primary system with a vertical particle damper. The parameters are $\mu = 0.1$, $\zeta = 0.012$, $\mu_s = 0.55$, dx/Z_{st}= 9, dy/Z_{st}=9, dz/Z_{st}=32, d/Z_{st}=1.5, e=0.75, A_0/Z_{st}=13, and 512 particles.

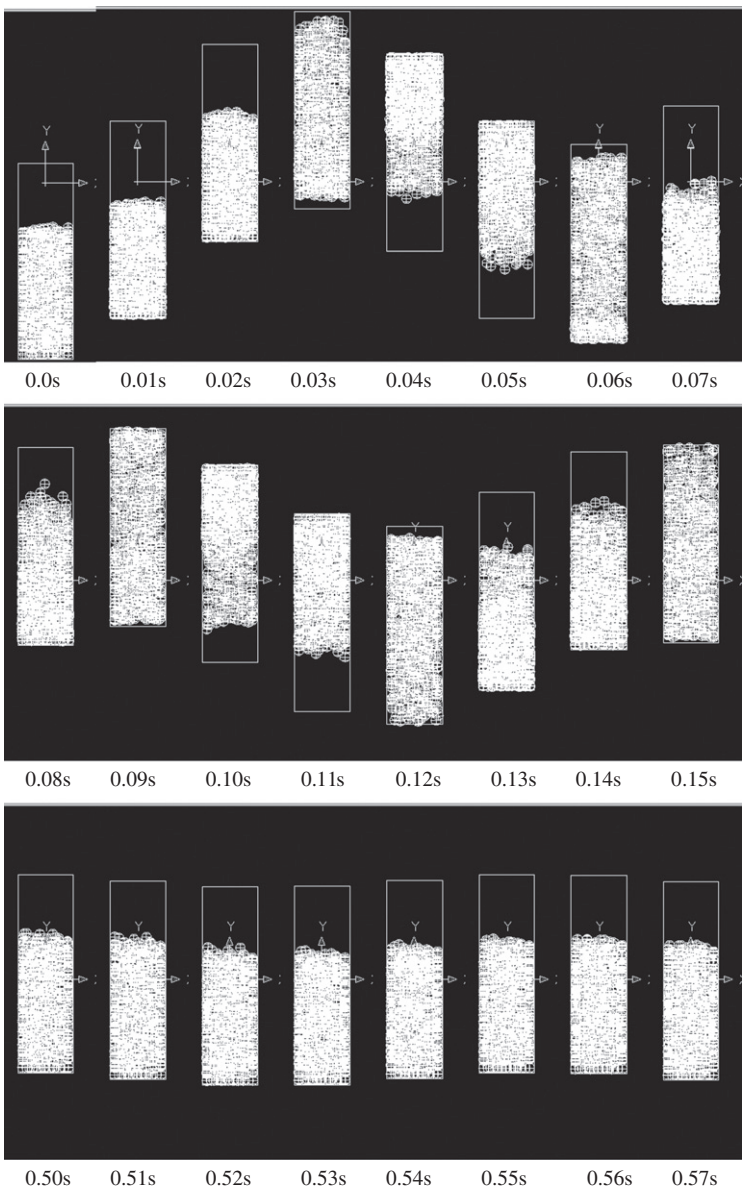

Fig. 4. Snapshots of the particles during free vibration of the damper, with the same parameters as in Fig. 3.

Fig. 3 shows the free vibration displacement of the primary system for an initial displacement (A_0). The displacement (Z) is normalized by dividing by the static deflection (Z_{st}). It clearly shows a dramatic attenuation of the transient vibration due to the presence of particles, and the equivalent damping ratio is increased from 0.012 to 0.048. Moreover, the natural frequency of the primary system becomes smaller because of the added particle mass.

Fig. 4 gives a series of snapshots to show the motion of the structural mass with the particles. These snapshots illustrate the approximate damping regimes during the course of free vibration [29]. In the first regime approximately between 0.0 and 0.05 s, the damper container walls impact the particles and transfer momentum to the particles. During the second regime, significant damping effect is achieved, not only due to a large number of collisions between particles and the container walls, but also to the mechanical energy dissipation through impact and friction. After this regime, the particles are nearly at rest relative to the container mass and little damping effect is observed. This is similar to the observations of the work done by the group led by Professor Poschel [40].

While the effect of the particle damping is clearly shown in Fig. 3, such damping is highly nonlinear. The ratio of root-mean-square (rms) value of the displacement of the primary system with a particle damper and that without a particle damper (σ_z/σ_{z0}) is used to quantify the vibration control effectiveness of the particle damper, which is also an indication of particle damping effect. Figs. 5 and 6 show that the particle damping depends on the vibration amplitude and the gap clearance, respectively. The optimum design strategies can be found in both cases. Consequently, it can be seen that a properly designed vertical particle damper could provide additional significant damping to the primary system, and

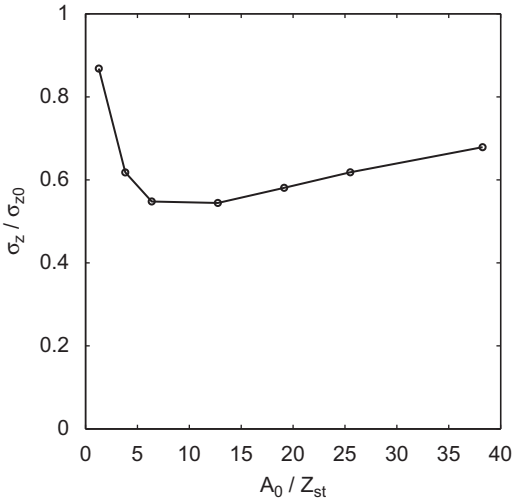

Fig. 5. RMS free vibration displacement response levels for the primary system with $\mu=0.1$, $\zeta=0.012$, $\mu_s=0.55$, dx/Z_{st}=9, dy/Z_{st}=9, dz/Z_{st}=32, d/Z_{st}=1.5, e=0.75, and 512 particles (effect of vibration amplitude).

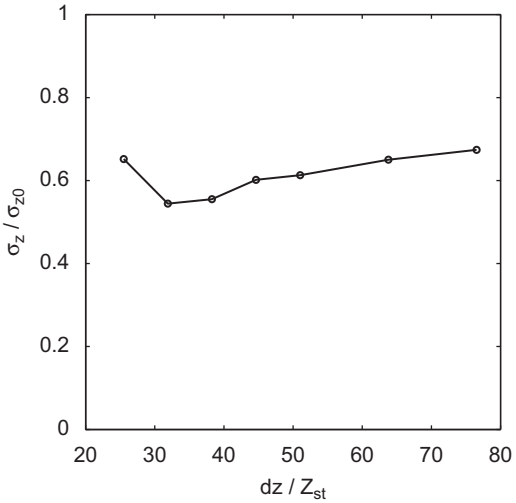

Fig. 6. RMS free vibration displacement response levels for the primary system with $\mu=0.1$, $\zeta=0.012$, $\mu_s=0.55$, dx/Z_{st}=9, dy/Z_{st}=9, d/Z_{st}=1.5, e=0.75, A_0/Z_{st}=13, and 512 particles (effect of clearance).

appreciably attenuate its response. Besides these two factors, many other parameters also influence the performance of particle dampers, and will be discussed in the following sections.

4. A particle damper with a SDOF system under multi-component random excitations

In this section, the performance of a horizontal particle damper attached to a SDOF system under two uncorrelated stationary random excitations, which are based on a normal (Gaussian) distribution with a bandwidth from zero to five times the primary system's natural frequency, is investigated. The model is shown in Fig. 1(c). Fig. 7 shows a sample rms response of the primary system in different container sizes, which displays a certain optimum operation. It can be seen that an operating time of about 1000 primary system's natural periods is sufficient for the primary system to reach a stationary condition.

In order to analyze and interpret the very complicated behavior of inter-particle as well as particle–container interactions, several "global" measures are presented to obtain some useful indices that can provide an overall indication of the performance of the damper, particularly as these measures relate to the optimum primary system response attenuation. It is found that the following quantities provide good "illumination" of the underlying complex physical phenomena occurring among the system components: (1) the *effective momentum exchange* and (2) the amount of internal energy dissipation due to impact and friction.

The collisions among interacting particle dampers can be separated into three types, according to the relative velocity of the particle and the primary system at the instant of impact:

1. Type 1: The absolute velocities of both particle and the primary system are opposite to each other at the instant immediately before contact, which is the face-to-face impact.
2. Type 2: Although the particle and the primary system's absolute velocities have the same direction, the relative velocity of the particle is opposite prior to contact, which is the case for the primary system catching up with the particle.
3. Type 3: The particle and system's absolute velocities and the particle's relative velocity have the same direction just before contact, which is the case for the particle catching up with the primary system.

Collisions of Type 1 and Type 2 can reduce the response of the primary system, because a collision force which is in the direction opposite to the velocity of the primary system tends to prevent its moving. This kind of momentum exchange can be defined as "beneficial momentum exchange" and this kind of impact can be called "beneficial impact". On the other hand, a collision of Type 3 is inclined to accelerate the primary system, thus such a type of momentum exchange is harmful to the response reduction of the primary system. Consequently, it is defined as "adverse momentum exchange" and the impact is defined as "adverse impact". A concept of "*Effective Momentum Exchange*" (*EME*) is proposed herein to conveniently describe the combined effects of a beneficial momentum exchange minus an adverse momentum exchange.

According to the contact force model in Section 2, the dissipated energy mainly has two sources, which are inelastic impacting and friction, and can be computed thus

$$E=\begin{cases}\sum\left(2\zeta_2\sqrt{mk_2}\dot{\delta}_n\dot{\delta}_n\,\mathrm{d}t+|F_{ij}^t\dot{\delta}_t\,\mathrm{d}t|\right) & \text{(particle}-\text{wall)}\\ \sum\left(2\zeta_3\sqrt{\dfrac{m_im_j}{m_i+m_j}k_3}\dot{\delta}_n\dot{\delta}_n\,\mathrm{d}t+|F_{ij}^t\dot{\delta}_t\,\mathrm{d}t|\right) & \text{(particle}-\text{particle)}\end{cases} \tag{12}$$

where dt is the contact time duration, and the dissipated energy is summed over all contact time durations.

Fig. 8(a) gives a general impression of how a particle damper is working within a range of container sizes, including lengths and widths (as the height does not influence the behavior very much, it is not included in this study). The length (dx)

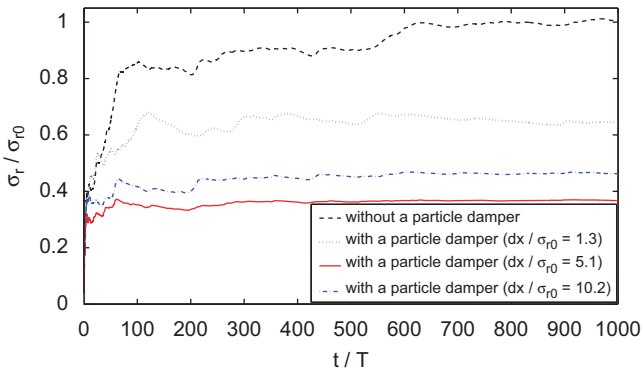

Fig. 7. RMS response time history of the displacement magnitude ($\sqrt{x^2+y^2}$) for the primary system with $\mu=0.108$, e=0.75, $\zeta=0.004$, $\mu_s=0.5$, $dy/\sigma_{r0}=3.8$, $d/\sigma_{r0}=0.8$ and 16 particles, under two simultaneous uncorrelated random excitations in the x and y directions.

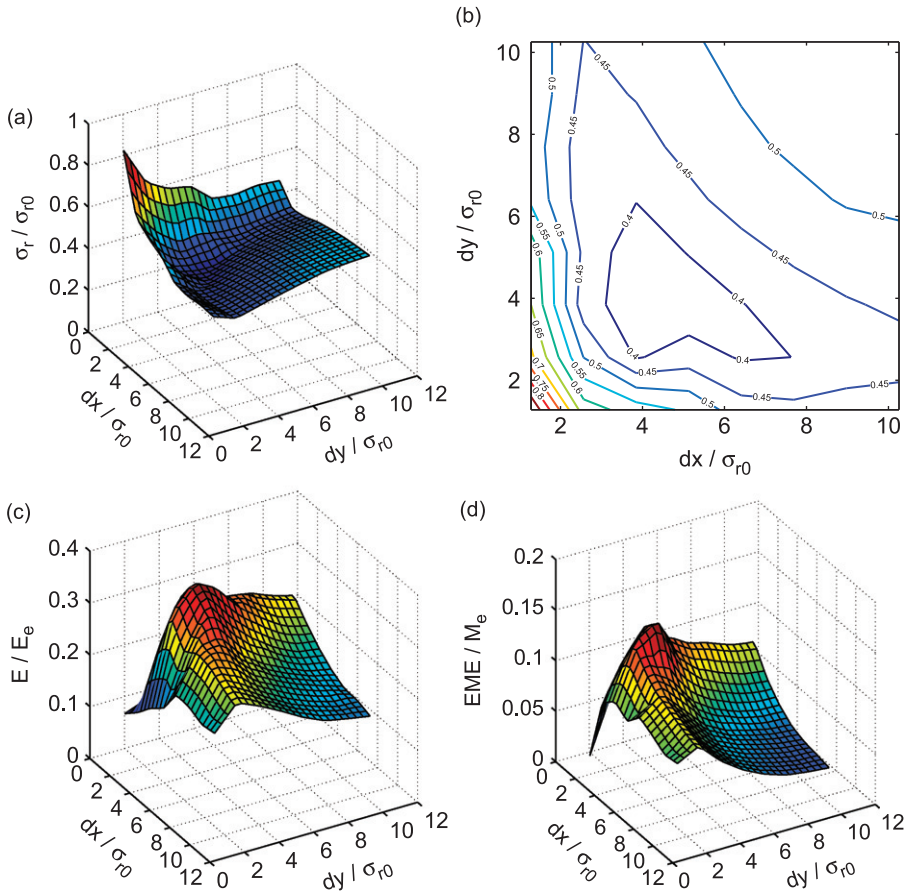

Fig. 8. (a) RMS displacement magnitude response levels; (b) Contour plot of σ_r/σ_{r0}; (c) Dissipated energy; (d) *Effective Momentum Exchange* for the primary system with $\mu = 0.108$, e=0.75, $\zeta = 0.004$, $\mu_s = 0.5$, $d/\sigma_{r0} = 0.8$ and 16 particles, under two simultaneous uncorrelated random excitations in the x and y directions.

is the separation of the walls of the damper in the x direction, and the width (dy) is the separation of the walls in the y direction, shown in Fig. 1(c). An optimum region, within which the primary system can get more than 60 percent reduction of the rms response, is clearly shown in the contour plot Fig. 8(b). In Fig. 8(c), the dissipated energy is plotted in dimensionless form by dividing the energy of the excitation force (E_e). One can find a high ratio of dissipation in the optimum region.

Similarly, a normalized version of the *Effective Momentum Exchange*, which is divided by the momentum exchange of the excitation force (M_e), is plotted in Fig. 8(d), and results in a relatively high value in the optimum range, too. The reasons for this behavior is that in small container sizes, the particles are piled together in many layers, which minimizes the motion of the lower layers, and only create a vigorous motion in the top-most layers. In large container sizes, the particles need to spend a long time transiting from one wall to the opposite wall, which leads to fewer impacts with the primary system; hence a trade-off exists, which is the reason why an optimum performance of the particle damper can be obtained.

5. A particle damper with a MDOF system

In this section, parametric studies of the performance of a horizontal particle damper attached to a 3DOF system under different dynamic loads are carried out to get a better understanding of the physics involved in particle dampers. The model can be found in Fig. 1(b). The natural frequencies of example primary system are f_1 = 1.58 Hz, f_2=4.44 Hz, and f_3=6.41 Hz, and the damping ratio is ζ = 0.01. The mode shapes corresponding to each natural frequency are shown diagrammatically in Fig. 9.

5.1. Free vibration

This simulation uses impulses at different storey locations to examine the effect of excitation input location. The duration of the impulse is considered to be very short and an initial velocity is exerted at different storey at the initial

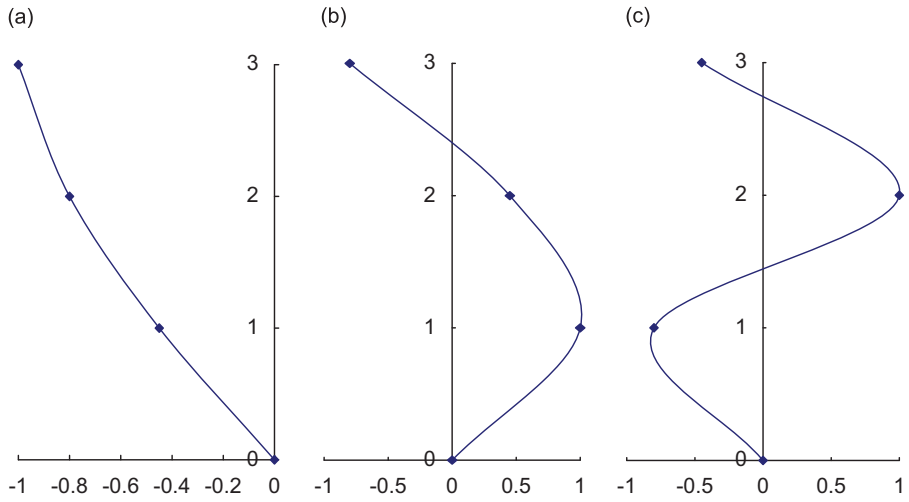

Fig. 9. Diagrammatic mode shapes of the primary system. (a) Mode1, (b) Mode2, and (c) Mode3.

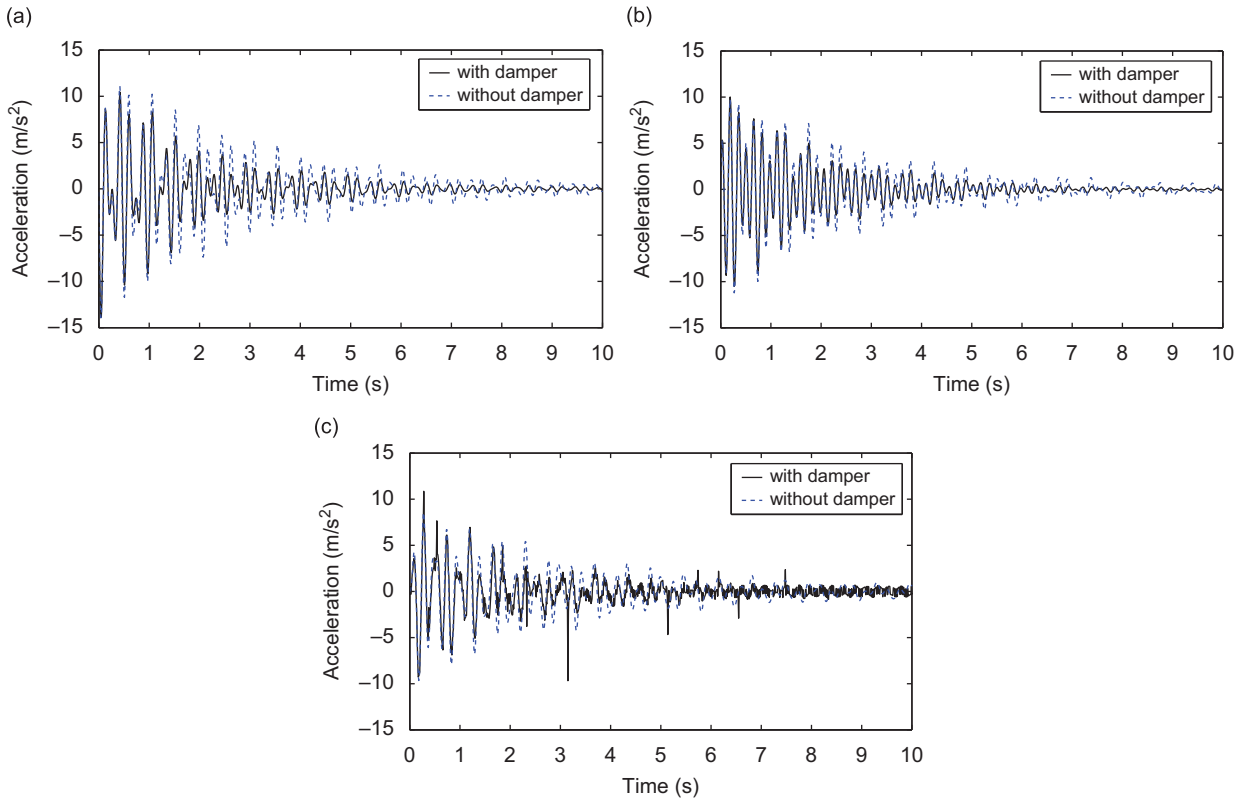

Fig. 10. Acceleration time histories of the (a) 1st floor, (b) 2nd floor, and (c) 3rd floor of the primary system, under excitation at the first storey.

instant. A single particle with a mass ratio (the fraction of particle mass and the whole primary system mass) of $\mu = 0.03$, a diameter of 25 mm, and a clearance of 60 mm is applied.

The response of the primary system with a particle damper decays much faster than that without damper. Figs. 10 and 11 show a sample acceleration and velocity time history of each floor under an impulse at the first floor. One can see that at the third floor, large accelerations are initiated as the impact mass collides with the stops, and then the impacts rapidly reduce the response of the structure at all floor levels. Once the motion of the third floor becomes insufficient for impacts to occur (which depends on the clearance, amplitude of motion and other parameters), the structure oscillates

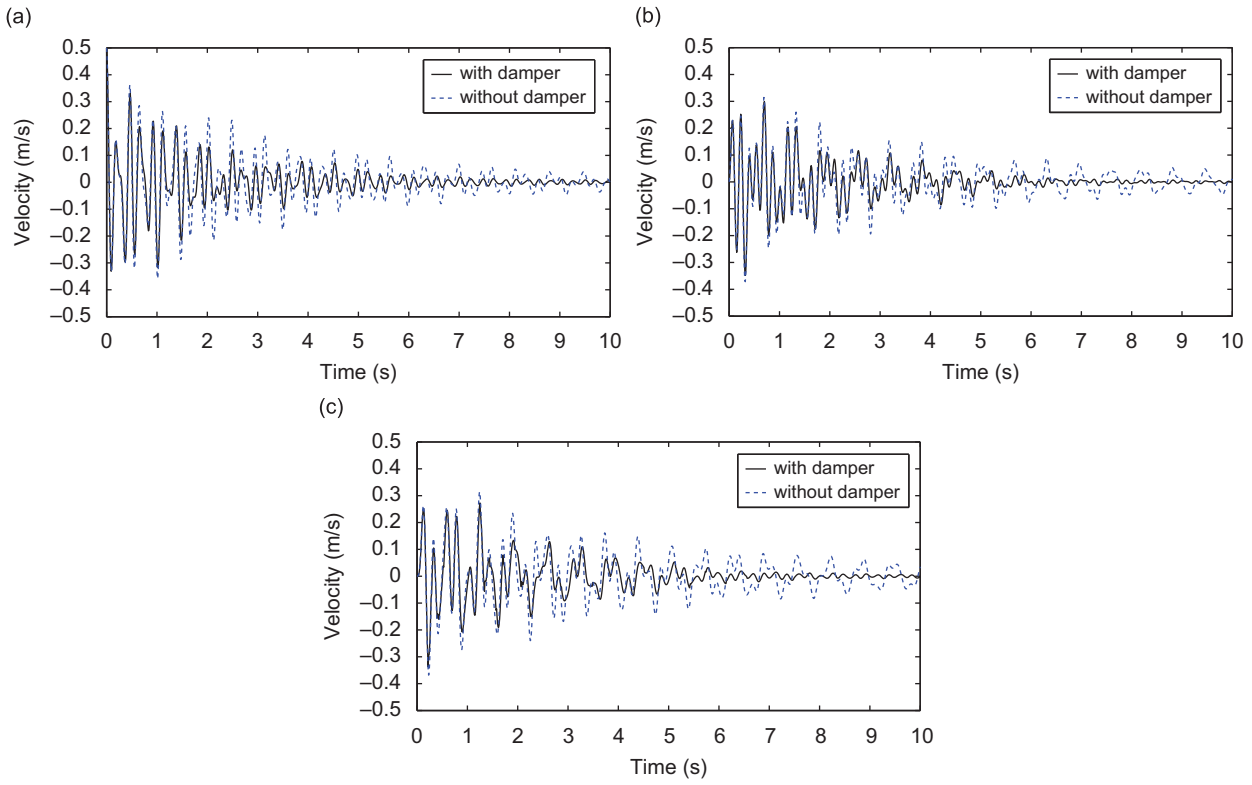

Fig. 11. Velocity time histories of the (a) 1st floor, (b) 2nd floor, and (c) 3rd floor of the primary system, under excitation at the first storey.

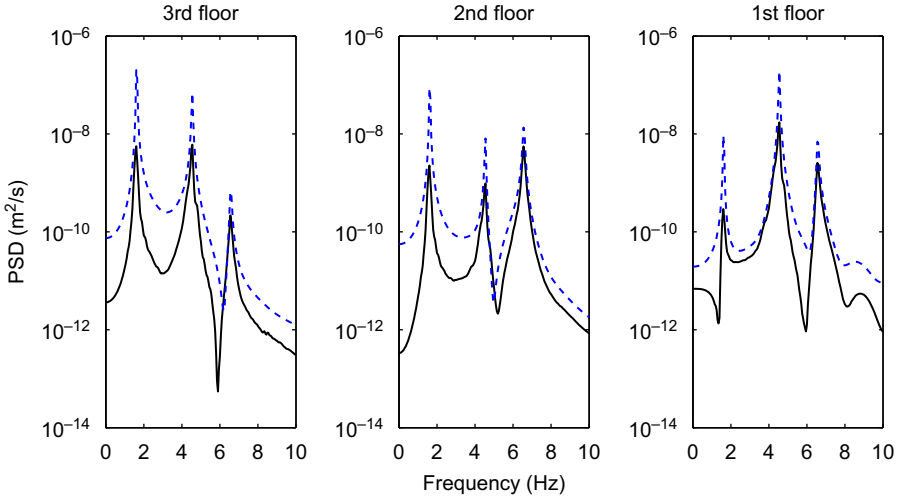

Fig. 12. Power spectral density of the primary system velocity response, under excitation at the first storey, in which the dotted line is the without-damper-case, while the solid line is the with-damper-case.

freely, with only internal damping of the structure itself causing the response to decay. Without the particle damper, there is no initial rapid reduction in response and the oscillations decay in a slow exponential form over a longer period of time, as shown by the dashed line. Moreover, it should also be noted that the acceleration of the third floor, where the impact damper is located, can be very high at the moment of collision, although these high accelerations are not evident in the response of the other storeys. As to the velocity response, there are no sudden changes at the instant of collision, and this is because velocity is the integral of accelerations.

Figs. 12–14 shows the corresponding power spectral density (PSD) of the velocity response, under the excitation force acting at the first, second, and third storey, respectively, in which the PSD is plotted in a logarithmic form for better

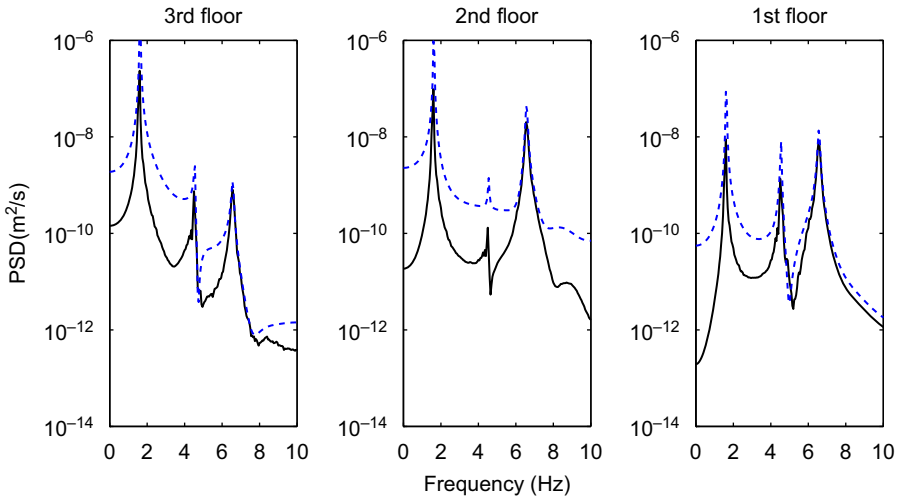

Fig. 13. Power spectral density of the primary system velocity response, under excitation at the second storey, in which the dotted line is the without-damper-case, while the solid line is the with-damper-case.

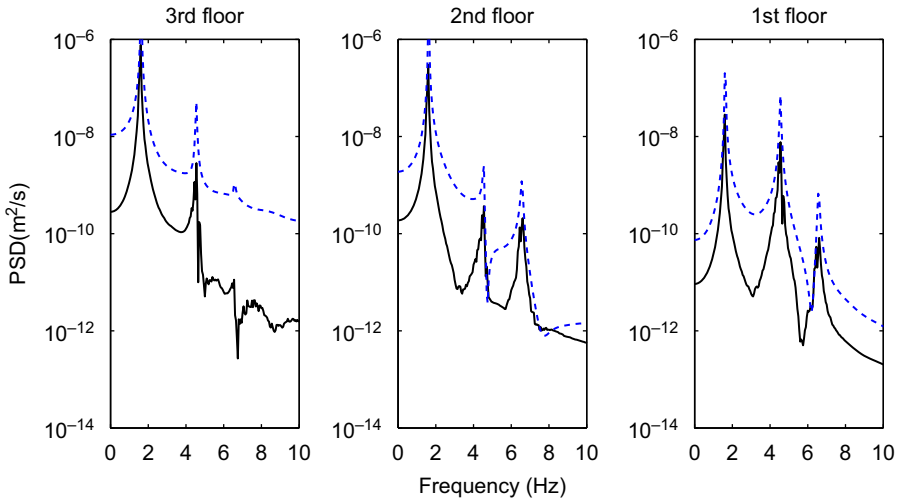

Fig. 14. Power spectral density of the primary system velocity response, under excitation at the third storey, in which the dotted line is the without-damper-case, while the solid line is the with-damper-case.

comparison. There is a clear vibration attenuating effect of the impact damper for each storey at the first mode of vibration regardless of the location of the excitation force; however, the vibration control effect upon the higher modes is more clearly affected by location of excitation. In particular, comparing Figs. 13 and 14, it can be observed that better control of the third mode of each storey occurs when excitation is at the third floor rather than at the second floor. One may also expect that the extent to which certain modes are excited depends on where the structure is excited, leading to a more obvious control effect where the response of the mode is greatly excited. The second mode is a clear example. It is greatly excited when the input force is at the first floor or third floor, as shown in Figs. 12 and 14; consequently, it is reasonably well controlled by the damper. On the other hand, it is excited very little when the input is at the second floor, as shown in Fig. 13. Due to this being the approximate location of an anti-node of the second mode shape; consequently, the controlling effect is not obvious. The above phenomena is also demonstrated in Li's experiments [19].

5.2. Stationary random excitation

In this part, different parameters, such as the mass ratio (μ), the coefficient of restitution (e), excitation levels, damping ratio of the primary system (ζ) and damper locations are investigated to get a broader view of the performance of particle dampers with a MDOF primary system. Since the percentage displacement reductions for all storeys have not much differences, to facilitate presentation, only the response of the first floor is demonstrated in the following figures.

Fig. 15 shows that increasing the mass ratio of particles can reduce the response of the primary system, but the reduction is not linearly proportional to the increase in the mass ratio; in fact, the effectiveness per unit mass ratio will decrease, in a nonlinear manner, as the mass ratio increases. Another interesting observation is that indefinitely increasing the mass of the particles may not reduce the response any further, especially for large container sizes. This phenomenon can be explained by considering the conservation of momentum between the particles and the system. As a specific particle's mass increases, its absolute velocity immediately after the impact decreases which, in turn, reduces its relative velocity, and it takes a longer time to travel towards the other wall of the container. The force of friction also contributes to the reduction in the velocity while the particle is in motion. As the mass is increased beyond a certain value, its relative velocity immediately after the impact does not allow it to overcome the frictional force while in motion, and it comes to rest relative to the system prior to reaching the other wall. At that point, if the system resumes its motion in the same direction and its acceleration is large enough to overcome the force of friction, the particle starts traveling in the opposite direction relative to the system. If a similar situation arises prior to reaching the other container's boundary, the particle reverses it direction once again. It is possible for the particle to reciprocate between the container's boundaries, while the system goes through several cycles of motion before making the next impact.

The coefficient of restitution e determines the rebound velocity of the particle and is the ratio between the relative velocity immediately following the impact to the relative velocity just prior to impact. It depends on the type, shape, and surface area of the materials coming in contact.

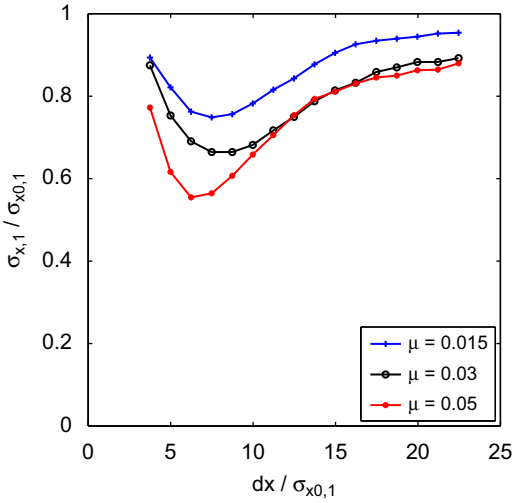

Fig. 15. RMS displacement response levels for the first storey of the primary system with damper on the third storey, e=0.75, $\zeta = 0.01$, $\mu_s = 0.5$, $dy/\sigma_{x0,1} = 7.5$, $d/\sigma_{x0,1} = 1.4$, and 10 particles (effect of mass ratio).

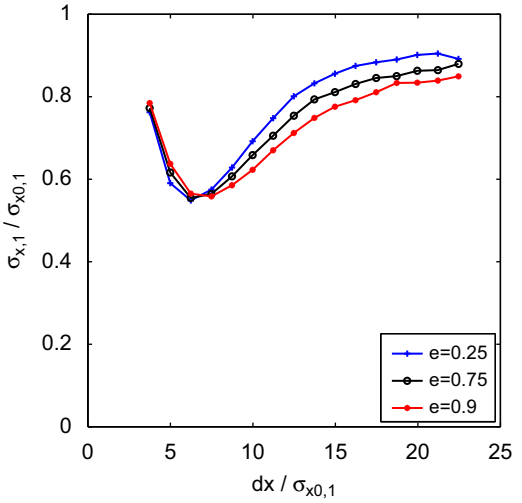

Fig. 16. RMS displacement response levels for the first storey of the primary system with damper on the third storey, $\mu = 0.05$, $\zeta = 0.01$ and $\mu_s = 0.5$, $dy/\sigma_{x0,1} = 7.5$, $d/\sigma_{x0,1} = 1.4$, and 10 particles (effect of coefficient of restitution).

Fig. 16 shows that higher e's lead to a more reduction in large-size containers, compared to lower e's. The reason for this behavior is that a higher e can result in a higher relative velocity immediately following the impact, which results in more collisions. Another significant observation that can be gleaned from Fig. 16 is that the sensitivity of a particle damper to changes in dx increases as e decreases, which results in a narrower optimum clearance for smaller e's. Consequently, a particle damper designed with a relatively high value of e can tolerate a broader range of excitation levels, while still performing around the optimum level.

Fig. 17 shows that the level of excitation plays a very important role. As the level of excitation increases, the efficiency of the damper increases due to the fact that the more energetic motion of the particles increase the exchange of momentum and dissipation of energy. On the other hand, when the excitation is high enough to mobilize all the particles, the response amplitude becomes independent of the intensity of the excitation, provided the dimensionless clearance ratio is maintained constant.

Fig. 18 shows that the efficiency of the particle damper increases with the damper "elevation" above the ground floor. This is because a higher storey has larger displacement, and it will impart more kinetic energy to the particles, which increases the amount of momentum exchange and energy dissipation.

Fig. 19 shows that the effectiveness of the particle damper increases as the primary system damping decreases. Consequently, the maximum effect of a particle damper would be achieved for a primary system with a negligible amount of inherent damping.

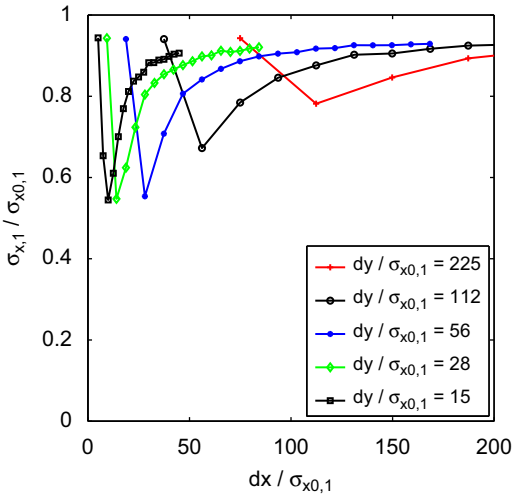

Fig. 17. RMS displacement response levels for the first storey of the primary system with damper on the third storey, $\mu = 0.05$, e=0.75, $\zeta = 0.01$, $\mu_s = 0.5$, and 10 particles (effect of excitation level).

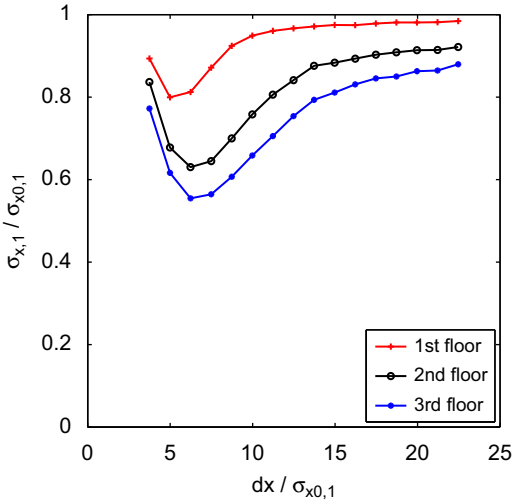

Fig. 18. RMS displacement response levels for the first storey of the primary system with $\mu = 0.05$, e=0.75, $\zeta = 0.01$ and $\mu_s = 0.5$, d$y/\sigma_{x0,1} = 7.5$, $d/\sigma_{x0,1} = 1.4$, and 10 particles (effect of damper location).

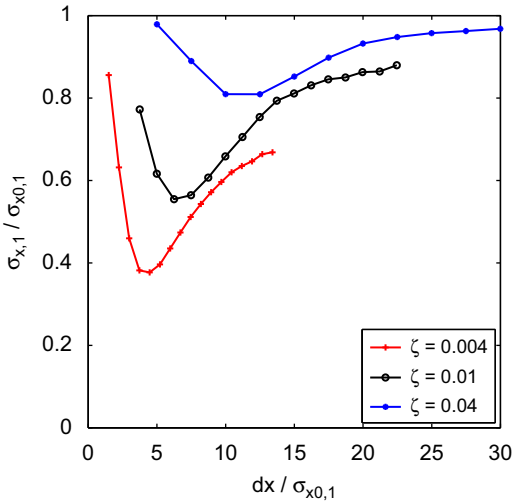

Fig. 19. RMS displacement response levels for the first storey of the primary system with damper on the third storey, $\mu = 0.05$, e=0.75, $\mu_s = 0.5$, and 10 particles (effect of primary system damping).

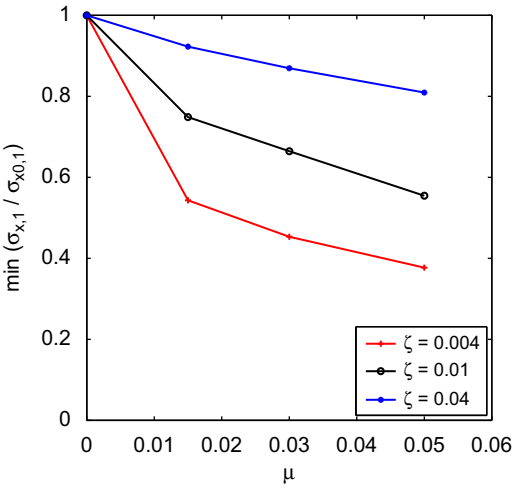

Fig. 20. Effect of primary system damping and mass ratio on the performance of particle damper with e=0.75, $\mu_s = 0.5$, and 10 particles.

Fig. 20 summarizes the effects of mass ratio and the primary system damping on the optimum performance of a particle damper. It is clear that, for a given ζ, the optimum response reduction is not a linear function of the mass ratio. Also, one can conclude that even with very small mass ratios, a properly designed particle damper is capable of substantial attenuation of the rms response level.

5.3. Nonstationary random excitation

In this part, the performance of particle dampers with a MDOF system under nonstationary excitation $s(t)$ is investigated. One convenient means of generating a synthetic nonstationary random excitation is to modulate a stationary random signal $n(t)$ through multiplication by a deterministic envelope function $g(t)$, as follows [41]:

$$s(t) = g(t)n(t) \tag{13}$$

$$g(t) = a_1 \exp(a_2 t) + a_3 \exp(a_4 t) \tag{14}$$

where $n(t)$ is the stationary random excitation, and $s(t)$ is the resulting nonstationary part. By a proper choice of a_1, a_2, a_3, and a_4, one can generate a variety of nonstationary excitations, such as earthquake-like excitations.

Simulations were done for the same system discussed in the previous section. The rms for the resulting non-ergodic process was computed by averaging over a large ensemble of records. For the case studied in this paper, the simulation

shows that the resulting rms will not change after the ensemble size approaches 200 records. Three different envelope functions ($g(t)$) were considered in this study, corresponding to a "fast", "medium", and "slow" rate of envelope decay.

Fig. 21 shows the effectiveness of the particle damper in reducing the rms response for three different envelope functions. For these three cases, the rms is calculated by averaging over 200 records, and the optimum gap clearance is chosen based on the maximum reduction in the peak value of the rms.

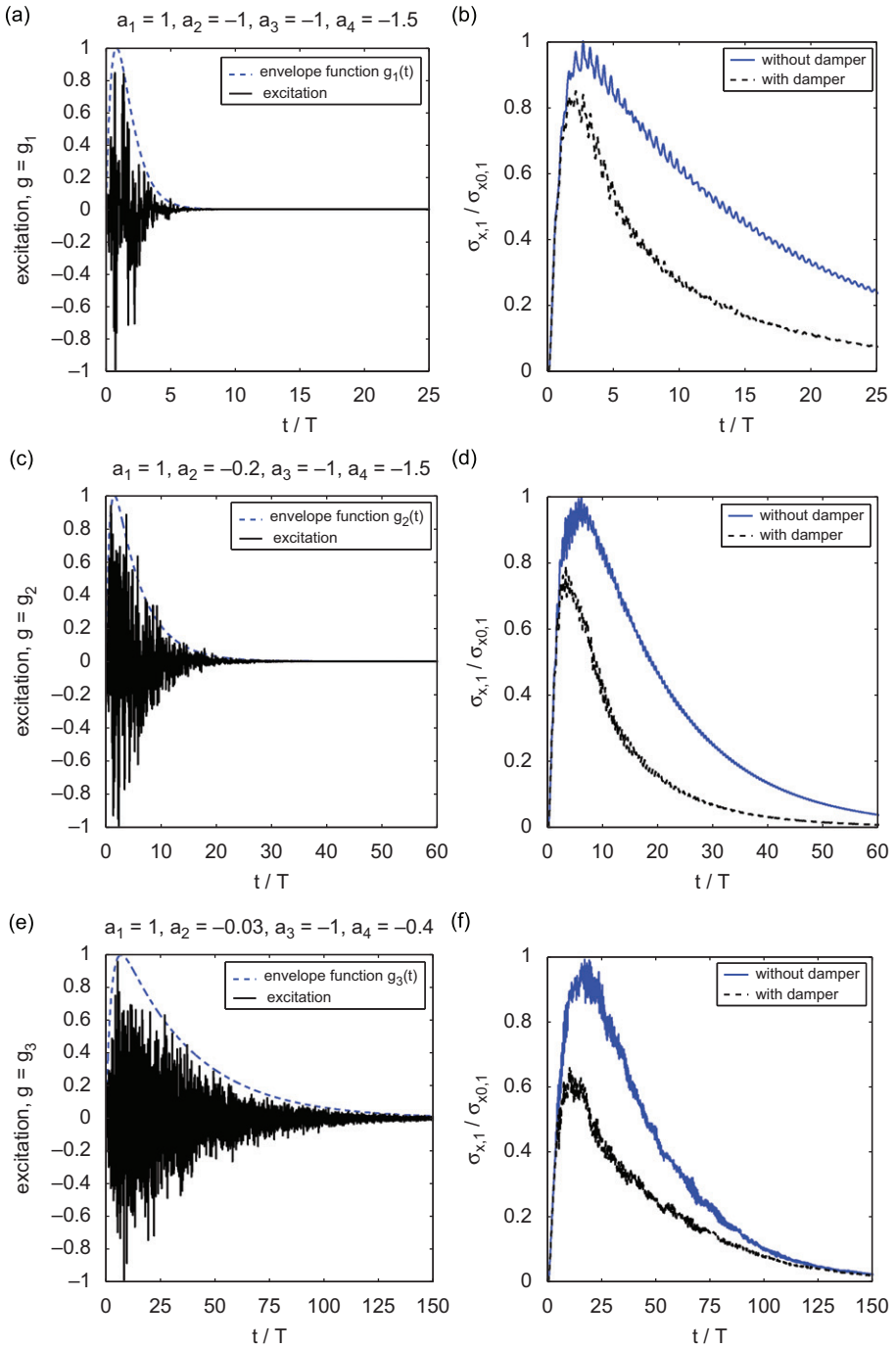

Fig. 21. (a,c,e) Exponential envelope function and the resulting nonstationary random excitation; (b,d,f) Transient rms displacement response levels for the first storey of the primary system with damper on the third storey, $\mu = 0.05$, $\zeta = 0.01$, e=0.75, dx=d_{opt}, $\mu_s = 0.5$, and 10 particles. (a–b) Excitation envelope: $g(t)$=$g_1(t)$=exp($-t$)−exp($-1.5t$), (c–d) Excitation envelope: $g(t)$=$g_2(t)$=exp($-0.2t$)−exp($-1.5t$), and (e–f) Excitation envelope: $g(t)$=$g_3(t)$=exp($-0.03t$)−exp($-0.4t$).

Table 1
Summary of the nonstationary simulation results for the first storey of the primary system.

Envelope function $g(t)$	Peak rms ratio $(\sigma_{\max,1}/\sigma_{0\max,1})$	Area under the rms time history $(\int \sigma_{x,1}\,dt/\int \sigma_{x0,1}\,dt)$
$g_1(t)$	0.85	0.54
$g_2(t)$	0.79	0.47
$g_3(t)$	0.66	0.61

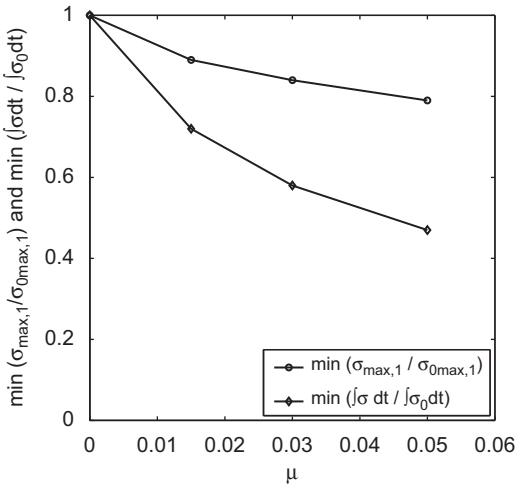

Fig. 22. Effect of mass ratio on the performance of particle damper in nonstationary random excitation with envelope function $g(t)=g_2(t)$. System parameters are $e=0.75$, $\zeta=0.01$, $\mu_s=0.5$, $dx=d_{opt}$, and 10 particles.

Table 1 presents the ratio of the peak rms $(\sigma_{\max,1}/\sigma_{0\max,1})$ and the ratio of the area under the rms time history $(\int \sigma_{x,1}\,dt/\int \sigma_{x0,1}\,dt)$ for the first storey of the primary system, for the three mentioned cases. One can conclude from the displayed results that a particle damper is significantly effective in reducing the area under the rms time history curve (which is an indication of the response "intensity"). However, the effectiveness of the particle damper in reducing the peak rms of the nonstationary response is not very significant, especially when the envelope function duration is short. One can find in Table 1 that, for $g(t)=g_1(t)$, the nonstationary excitation duration is about 25 natural periods of the system, and the resulting reduction in the peakrms is only about 15 percent, while the reduction in the area under the rms time history is about 46 percent. The reason for this behavior is due to the particle damper nature: it takes a while for the particles to acquire enough momentum for effective vibration attenuation. By increasing the envelope duration, the behavior of the particle damper improves and gets closer to the stationary one. For example, for $g(t)=g_3(t)$, the nonstationary excitation duration is about 150 natural periods of the system, and the resulting reduction in the peak rms is about 34 percent, which is closer to what is achieved for the same situation in the stationary excitation case (Fig. 20 shows about 42 percent reduction in the stationary rms with similar system parameters).

Fig. 22 summarizes the performance of a particle damper in reducing the ratio of the peak rms, and the area under the rms time history curve, for different mass ratios.

On the other hand, one can relate the peak transient rms $(\sigma_{\max})$ to the actual peak response (x_{peak}). Fig. 23 shows the probability density and cumulative distribution of the actual peak response for more than 200 ensembles. From this figure, one can conclude that with more than 98 percent confidence, the actual peak response is less than three times the transient rms peak $(P(x_{1,\text{peak}} < 3\sigma_{x1,\max}) > 98)$ percent. Therefore, the information about the statistics of the actual peak response is embedded in the transient rms plot.

6. Summary and conclusions

Even though several previous studies of particle dampers have been reported in the literature, currently there are no satisfactory guidelines for determining the optimum design strategy for maximizing the performance (i.e., response attenuation capability) of this class of highly nonlinear dampers when attached to a primary system subjected to broad-band random excitations.

This paper first investigated the performance of a vertical particle damper under free vibration, then a particle damper with a SDOF primary system under multi-component random excitations, and finally the behavior of a particle damper

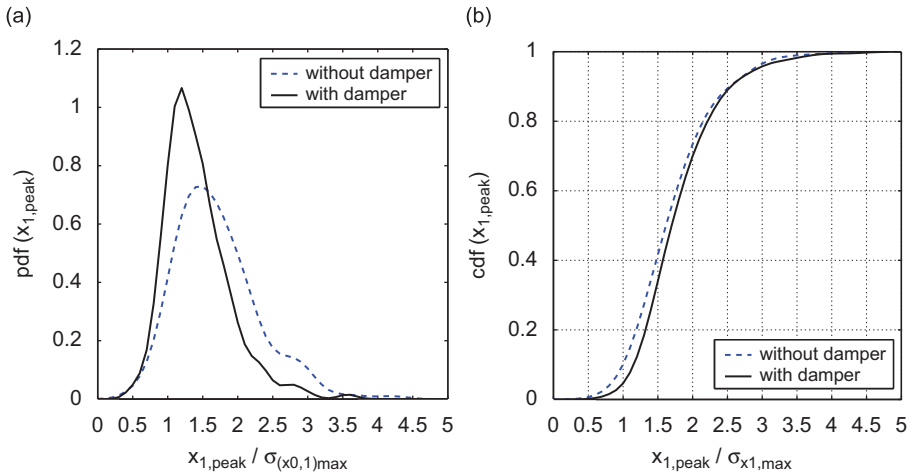

Fig. 23. (a) Probability density, and (b) Cumulative distribution of the actual peak response for the first storey of the primary system with damper on the third storey, under the nonstationary random excitation with the envelope function $g(t)=g_2(t)$. System parameters are $\mu=0.05$, $\zeta=0.01$, e = 0.75, dx = d_{opt}, $\mu_s=0.5$, and 10 particles. Based on CDF plot, one can observe that $P(x_{1,peak}<3\sigma_{x1,max})>98$ percent.

attached to a MDOF primary system under dynamic loads. Optimum operating regions are all determined and two "global" indices (the *effective momentum exchange* and the amount of internal energy dissipation due to impact and friction) are shown to be suitable measures to indicate this optimum performance.

Using well-established discrete particle modeling approaches, all significant interaction forces among the particles and with the rigid walls of their container are properly accounted for, including sliding friction, gravitational forces, and oblique impacts. This numerical method helps to provide information of particle motions during vertical vibrations, which can be divided into three different regions, and also helps to explain the associated damping characteristics.

For a MDOF primary system, the first mode can be effectively controlled by a properly designed particle damper; however, the higher modes are more affected by other parameters. The location of the input to the structure results in different degrees of damping. The reason may lie in the change in modal response of the structure, and hence the change in motion of the storey where the impact damper is located.

Extensive parametric studies are presented to evaluate the influence of various system parameters such as: mass ratio, primary system damping, coefficient of restitution, container dimensions, excitation amplitude and components, input locations and damper locations. It is shown that properly designed particle dampers (vertical and horizontal) can significantly attenuate the response of lightly-damped primary systems (SDOF and MDOF) that are subjected to dynamic loads (free vibration, stationary random excitation, as well as nonstationary random excitation, with single component or multi-component).

Acknowledgements

Financial supports from the National Natural Science Foundation of China through Grant 90815029 is highly appreciated.

References

[1] D. Zhao, A. Morgans, Tuned passive control of combustion instabilities using multiple helmholtz resonators, *Journal of Sound and Vibration* 320 (4–5) (2009) 744–757.
[2] M. Franchek, M. Ryan, R. Bernhard, Adaptive passive vibration control, *Journal of Sound and Vibration* 189 (5) (1996) 565–585.
[3] P. Gardonio, S. Elliott, Passive and active isolation of structural vibration transmission between two plates connected by a set of mounts, *Journal of Sound and Vibration* 237 (3) (2000) 483–511.
[4] D. Guyomar, A. Badel, Nonlinear semi-passive multimodal vibration damping: an efficient probabilistic approach, *Journal of Sound and Vibration* 294 (1–2) (2006) 249–268.
[5] S. Masri, T. Caughey, On the stability of the impact damper, *Journal of Applied Mechanics* 33 (3) (1966) 586–592.
[6] A. Paget, Vibration in steam turbine buckets and damping by impact, *Engineering* 143 (1937) 305–307.
[7] P. Lieber, An acceleration damper: development, design and some application, *Transactions of the American Society of Mechanical Engineers* 67 (1945) 523–530.
[8] S. Masri, Effectiveness of two-particle impact dampers, *Journal of the Acoustical Society of America* 41 (6) (1967) 1553–1554.
[9] S. Masri, Analytical and experimental studies of multiple-unit impact dampers, *Journal of the Acoustical Society of America* 45 (5) (1969) 1111–1117.
[10] S. Masri, General motion of impact dampers, *Journal of the Acoustical Society of America* 47 (1P2) (1970) 229–237.
[11] C. Bapat, S. Sankar, Multiunit impact damper—reexamined, *Journal of Sound and Vibration* 103 (4) (1985) 457–469.
[12] C. Bapat, Periodic motion of an impact oscillator, *Journal of Sound and Vibration* 209 (1) (1998) 43–60.

[13] N. Popplewell, S. Semercigil, Performance of the bean bag impact damper for a sinusoidal external force, *Journal of Sound and Vibration* 133 (2) (1989) 193–223.
[14] L. Bryce, M. Eric, E. Steven, Effectiveness and predictability of particle damping, *Smart Structures and Materials 2000: Damping and Isolation* 3989 (1) (2000) 356–367.
[15] X. Bai, B. Shah, L. Keer, Q. Wang, R. Snurr, Particle dynamics simulations of a piston-based particle damper, *Powder Technology* 189 (1) (2009) 115–125.
[16] M. Thomas, The impact damper as a method of improving cantilever boring bars, *Journal of Engineering Industry ASME* 2 (1975) 859–866.
[17] S. Ema, E. Marui, A fundamental study on impact dampers, *International Journal of Machine Tools and Manufactures* 34 (3) (1994) 407–421.
[18] Y. Michael, A. George, A. Stephen, H. Gary, Development of a design curve for particle impact dampers, *Smart Structures and Materials 2004: Damping and Isolation* 5386 (2004) 450–465.
[19] K. Li, A. Darby, Experiments on the effect of an impact damper on a multiple-degree-of-freedom system, *Journal of Vibration and Control* 12 (5) (2006) 445–464.
[20] A. Papalou, S. Masri, Performance of particle dampers under random excitation, *Journal of Vibration and Acoustics—Transactions of the ASME* 118 (4) (1996) 614–621.
[21] A. Papalou, S. Masri, Response of impact dampers with granular materials under random excitation, *Earthquake Engineering & Structural Dynamics* 25 (3) (1996) 253–267.
[22] A. Papalou, S. Masri, An experimental investigation of particle dampers under harmonic excitation, *Journal of Vibration and Control* 4 (4) (1998) 361–379.
[23] W. Liu, G. Tomlinson, J. Rongong, The dynamic characterisation of disk geometry particle dampers, *Journal of Sound and Vibration* 280 (3–5) (2005) 849–861.
[24] Z. Xu, K. Chan, W. Liao, An empirical method for particle damping design, *Shock and Vibration* 11 (5–6) (2004) 647–664.
[25] X. Fang, J. Tang, Granular damping in forced vibration: qualitative and quantitative analyses, *Journal of Vibration and Acoustics—Transactions of the ASME* 128 (4) (2006) 489–500.
[26] C. Wu, W. Liao, M. Wang, Modeling of granular particle damping using multiphase flow theory of gas-particle, *Journal of Vibration and Acoustics—Transactions of the ASME* 126 (2) (2004) 196–201.
[27] M. Saeki, Impact damping with granular materials in a horizontally vibrating system, *Journal of Sound and Vibration* 251 (1) (2002) 153–161.
[28] M. Saeki, Analytical study of multi-particle damping, *Journal of Sound and Vibration* 281 (3–5) (2005) 1133–1144.
[29] K. Mao, M. Wang, Z. Xu, T. Chen, Dem simulation of particle damping, *Powder Technology* 142 (2–3) (2004) 154–165.
[30] L. Hu, Q. Huang, L. ZX, A non-obstructive particle damping model of dem, *International Journal of Mechanics and Materials in Design* 4 (1) (2008) 45–51.
[31] C. Wong, M. Daniel, J. Rongong, Energy dissipation prediction of particle dampers, *Journal of Sound and Vibration* 319 (1–2) (2009) 91–118.
[32] P. Cundall, O. Strack, A distinct element model for granular assemblies, *Geotechnique* 29 (1979) 47–65.
[33] Y. Du, S. Wang, Energy dissipation in normal elastoplastic impact between two spheres, *Journal of Applied Mechanics* 76 (2009).
[34] T. Elperin, E. Golshtein, Comparison of different models for tangential forces using the particle dynamics method, *Physica A* 242 (3–4) (1997) 332–340.
[35] A. Di Renzo, F. Di Maio, Comparison of contact-force models for the simulation of collisions in dem-based granular flow codes, *Chemical Engineering Science* 59 (3) (2004) 525–541.
[36] S. Masri, A. Ibrahim, Response of the impact damper to stationary random excitation, *The Journal of the Acoustical Society of America* 53 (1) (1973) 200–211.
[37] S. Masri, Steady-state response of a multidegree system with an impact damper, *Journal of Applied Mechanics—Transaction of the ASME* 40 (1) (1973) 127–132.
[38] Z. Lu, S. Masri, X. Lu, Parametric studies of the performance of particle dampers under harmonic excitation, *Structural Control and Health Monitoring* 9999 (2009) doi:10.1002/stc.359.
[39] R. Friend, V. Kinra, Particle impact damping, *Journal of Sound and Vibration* 233 (1) (2000) 93–118.
[40] C. Saluena, T. Poschel, S. Esipov, Dissipative properties of vibrated granular materials, *Physical Review E* 59 (4) (1999) 4422–4425.
[41] S. Masri, Response of multidegree-of-freedom system to nonstationary random excitation, *Journal of Applied Mechanics* 45 (3) (1978) 649–656.